Application of Gravity Current Model to Analysis of Squall-Line Gust Front

JESS CHARBA[1,2]

Techniques Development Laboratory, NOAA, Silver Spring, Md. 20910

ABSTRACT

An analysis of a severe gust front is made to examine its three-dimensional structure. The data used are from the storm measurement network operated by the National Severe Storms Laboratory (NSSL). The important structural features shown in the analysis include: i) intense wind and thermal gradients at the leading edge of the air mass; ii) retardation of the cold-air front near the ground; and iii) vertical protrusion of the cold air to 1700 m at the front of the cold air mass, forming a bulge called a head. Upstream of the head, the depth of the cold air was almost constant at 1350 m; iv) a well defined circulation cell with a horizontal axis was found within the head; this wind field was associated with a core of maximum horizontal wind speed of 34 m sec^{-1} only 175 m above the ground, upward motion of 5–10 m sec^{-1} within the frontal zone, and weaker downward motion on the rear side of the head. In these structural characteristics, as well as in some substructural properties, this gust frontal air mass is found to be similar to laboratory-produced gravity currents. Moreover, the horizontal displacement speed of the gust front agrees with empirical and dynamical theory of gravity currents.

1. Introduction

This study concerns the cold air mass that flows outward from beneath intense thunderstorms. This air mass is often characterized by destructive surface wind gusts; for this reason its leading edge is called a gust front.

Various facets of the gust frontal structure have been documented. Byers and Braham (1949) described the surface wind field using high-density, surface mesonetwork data. Fujita (1967) examined the turbulence structure of a squall line gust front from flight recordings of commercial aircraft, flying through the squall line in the layer 2,500–7,000 ft. Florida thunderstorm outflows were analyzed by Goldman and Sloss (1969) using high resolution measurements from the 150-m NASA tower. Barclay and Wilk (1970) and Colmer (1971) analyzed wind measurements of Oklahoma gust fronts from the surface mesonetwork and the 444-m instrumented tower operated by the National Severe Storms Laboratory (NSSL).

There remains a need to define further the structure of the gust-frontal air mass. Lacking most is knowledge of the small-scale wind and thermal fields above the ground. It is commonly believed that the intense wind shears that characterize a well-formed gust front may constitute a serious hazard to low-flying aircraft; the danger is thought greatest for aircraft in landing and take-off maneuvers. Better understanding of the gust front would benefit those responsible for evaluation of the hazard. We also need to improve short-period forecasts of the gust front for better warnings, particularly around airports.

The main focus of this study is on the small-scale analysis of the wind and thermal field of the gust front in three spatial dimensions. All pertinent data gathered by NSSL was analyzed for a squall line gust front passing over the NSSL network near midnight of 31 May–1 June 1969 (see Barnes *et al.*, 1971, for a complete description of the network). On this date property and crop damage occurred over a large portion of Central Oklahoma; therefore, we felt it would be valuable to analyze this gust frontal case.

We also examined the physics of this cold air mass by comparing its structure with that of gravity currents; we refer to the laboratory experiments of Keulegan (1958), Middleton (1966), and Simpson (1969, 1972) for a model gravity-current structure. The driving force of the cold air mass was also studied by comparing its measured horizontal speed with that it would have if it were propagating as a gravity current; this is done by comparing the gust front's forward speed with that predicted from applications of empirical and dynamical theory of gravity currents (von Kármán, 1940; Keulegan, 1958; and Benjamin, 1968).

2. History of gust front

The squall line that produced the severe gust front in central Oklahoma near midnight of 31 May–1 June 1969 began to develop in northwestern Oklahoma and southwestern Kansas near 1800 CST, 31 May (Fig. 1a).

[1] This article is a condensed version of a Ph.D. thesis submitted to the Graduate College of the University of Oklahoma.

[2] This study is reported in more detail in Charba and Sasak. (1971b) and Charba (1972).

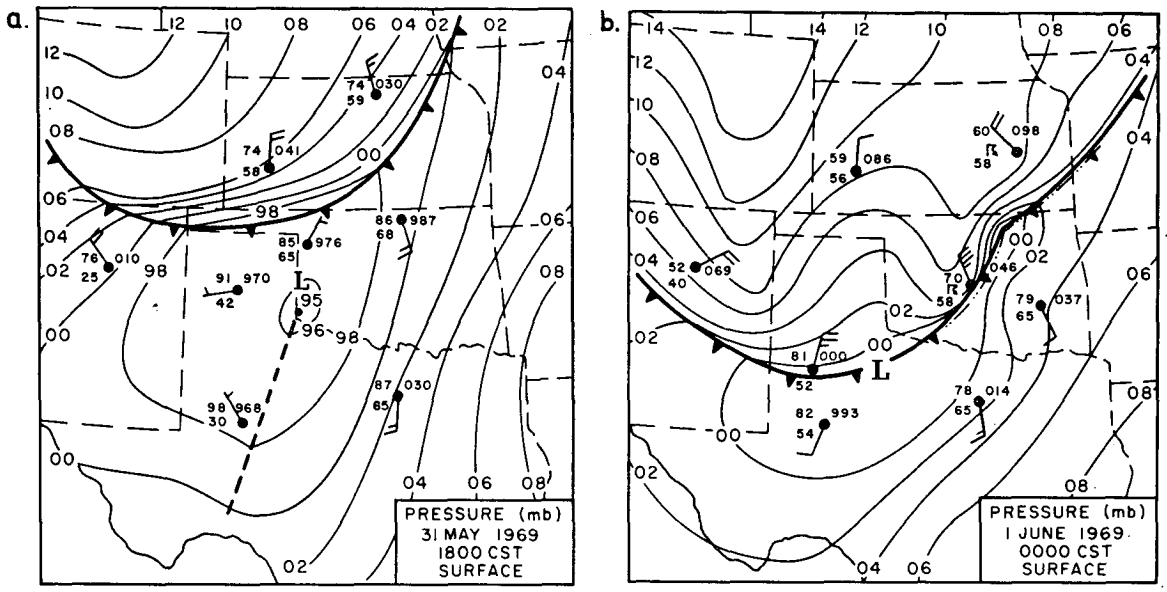

FIG. 1. Regional surface maps. Solid lines are isobars drawn at 2-mb intervals. The heavy dashed line in (a) is a pressure trough. The squall line appears in (b) as the dash-dot line. At the selected stations, plotted temperatures and dew points are in °F and a whole wind barb equals 10 kt.

By 0000 CST, a small wave had developed on the cold front; the squall line is seen to lie just ahead of the cold front in the neighborhood of the wave.

The gust front that preceded the heavy precipitation echoes of the squall line stretched across the center of the NSSL surface-station network at 2337:30 CST (see Figs. 2 and 3). A time sequence of WSR-57 radar echo pictures (not shown) revealed a "thin line echo" advancing southeastward ahead of a large storm echo. This echo is labeled A in Fig. 3; the thin line echo is the arc-shaped figure outlined by the dotted line. During the time the thin line was within the network, its position was generally coincident with the forward edge of the outflow from echo A. This correspondence was used to reconstruct the history of the gust front's forward movement before it entered the sampling network.

We found that the southeastward movement of the gust front was practically unchanging as it entered and passed over the network during the period 2313:30 CST to 2358:30 CST; its speed was 21 m sec^{-1}. Although echo A's speed was at least 2 m sec^{-1} less during this period, its size and reflectivity changed little.

These facts show that the cold air mass, whose leading edge had spread about 20 km ahead of echo A, was basically steady in forward movement and stage of development as it engulfed the network area (see Byers and Braham 1949). This temporal steadiness and the rather large areal coverage of the damaging winds (see Charba, 1972) made this case ideal for intensive analytical study.

3. Data analysis procedures

a. Data types

The data used to "reconstruct" the gust frontal air mass were from NSSL's high density network of surface stations and the WKY-TV transmitting tower, instrumented to 444 m (Fig. 2). Wind and temperature measurements were automatically recorded on strip charts.

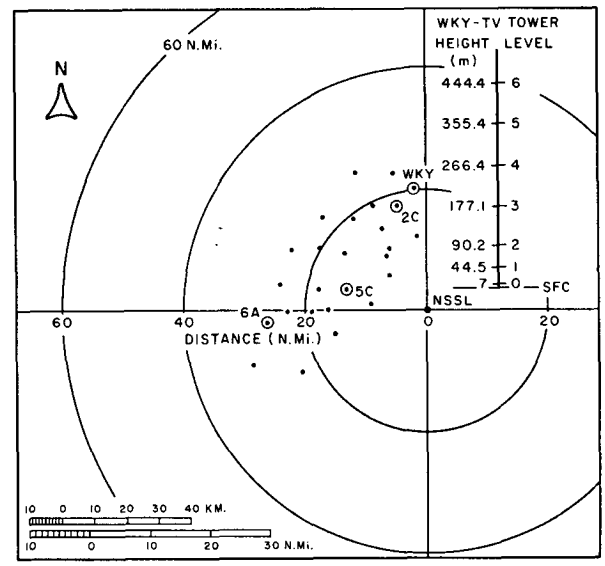

FIG. 2. Surface station network (dots) and instrumented WKY-TV tower operated by NSSL in 1969. The inset at the upper right of the figure shows the instrumented levels of the tower. Concentric circles are range markers of the WSR-57 radar located at NSSL.

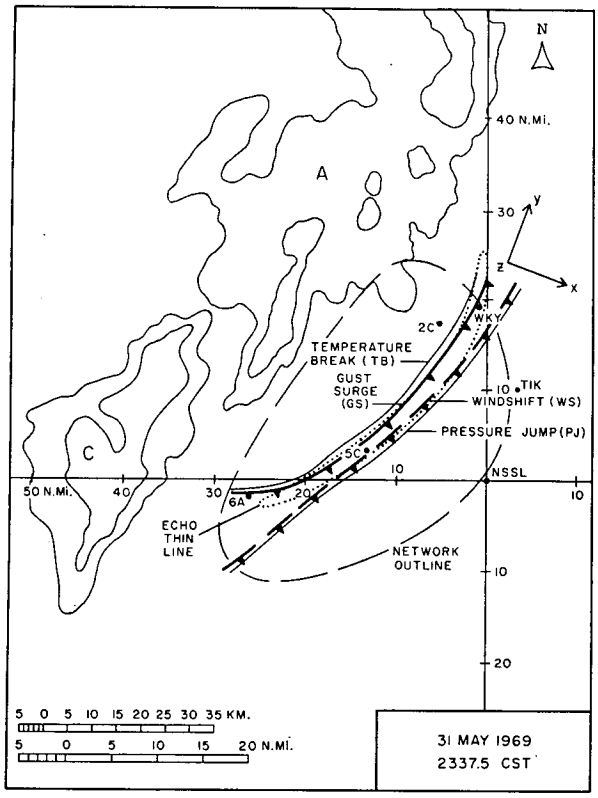

FIG. 3. Schematic of significant features appearing in the analysis of the 31 May 1969 squall line at 2337:30 CST. The radar echo contours represent the 2×10^{1} mm^{6} m^{-3} and 2×10^{4} mm^{6} m^{-3} reflectivity isoplets. The large-dashed line encloses the surface station network shown in Fig. 2. In Section 3 of the text we demonstrate that the gust surge (initial strong gust) and the temperature break (sharp temperature fall) lines shown in the figure define the leading edge of the gust front. The windshift (wind direction shift) and pressure jump (abrupt pressure rise) were related to a separate phenomenon.

In addition to wind and temperature, the surface stations also recorded pressure and relative humidity. NSSL maintenance personnel calibrated the surface recording equipment once a week. After objectively derived corrections were applied to the strip charts the accuracy of recorded variagles approach standards of the National Weather Service. The accuracy of the wind and temperature measurements from the TV-tower (Carter, 1970) easily exceeded the requirements for the analysis with no corrections necessary.

b. Data processing and analysis

To retain the sharp gradients and other important small-scale features of the gust frontal air mass, we set about to analyze for wavelengths as small as 10 km. Since the average surface station spacing was about 9 km, we had to extrapolate the data to points between stations using the time-to-space conversion technique (Fujita, 1963). The technique was also applied to the tower records for constructing vertical cross sections through the gust front.

The "raw" strip chart traces contained sizable wiggles from waves of less than 10-km wavelength. These are generally non-systematic and must be removed. Therefore, smoothing was applied to remove periods $\leq$5.0 min (or wavelengths $\leq$6 km). This smoothing was applied directly to the traces by a manual process, except in the case of the pressure, where a 3-point "hanning" filter was applied to data abstracted at 2.5-min intervals.

Plotted data fields were analyzed both at the surface and in an x–z plane up to 444 m. The x direction is normal to the leading edge of the gust front as shown in Fig. 3.

c. Special computations

A few of the parameters analyzed were derived from the raw data after special computations were made. The procedure for computing the streamfunction and gustiness of the wind and the surface pressure field are briefly described.

Following the procedure discussed by Clarke (1961), the streamfunction, ψ, in the x–z plane is computed from

$$\psi = -\int_0^h u\,dz$$

where u is the wind component in the x-direction and h is height. The actual flow in this plane is well approximated by this ψ pattern if

$$\frac{\partial u}{\partial x} \Big/ \frac{\partial v}{\partial y} \gg 1 \qquad (1)$$

where v is the y-component of the wind. The validity of Eq. (1) for this particular case is discussed later.

The gustiness of the wind was obtained from the wind charts after two curves were sketched on each wind trace. One smooth curve was sketched to pass through the speed peaks; a similar curve was drawn for the minimum speed points. The speed difference between these curves defined the wind gustiness.

The method used to represent the surface pressure field was to express the station pressure as a mesoscale deviation from the large scale pattern. Simple band-pass filtering was applied objectively to abstracted microbarogram data sets to separate the mesoscale periods from other periods. The smooth curve representing the large-scale pressure change at a station has been called the pressure trend by Charba and Sasaki (1971a).

d. Information presentation schemes

During the data plotting and analysis a great deal of care was taken to properly position extrapolated data to points between stations and to cross-check small-scale features appearing in different analyzed fields. For example, when the same variable was

analyzed both over the network and in a vertical cross section (z–x plane) care was taken to ensure that small change variations appeared in both fields and at the same point in space. Likewise, during analyses of the surface network data fields, the strip chart records of selected stations were transformed to space sections and superposed on the network charts to ensure that the two were consistent.

The analyzed fields and schematics depicting the structure of the gust front are shown in Figs. 4–8. As an aid in tracing small-scale features from one chart to the next, we inserted labeled markers. Note that the surface network fields (Figs. 4a, 4c, etc., and Figs. 6a and 7) contain the line segments A_1B_1, . . . A_4B_4. These are section lines; they refer to the identically labeled segments of the spatial sections in Fig. 5. For a particular variable, significant points evident in corresponding fields are tagged by X-marks and labeled as shown.

A similar tracing scheme was used to relate the surface network patterns with features appearing in the vertical section fields of wind and temperature (Figs. 4b, 4d, etc., and Fig. 6b). The lateral boundaries of these vertical sections, labeled X and Y, are located on the section line A_1B_1 of the surface network fields. Structural elements that are common to both fields are indicated by X-marks and labeled in lower case letters.

4. Three-dimensional structure of the gust front

a. Structure below 444 m

Tepper (1950) has given a detailed description of the weather changes that typify the arrival of an intense squall line system at the ground. He found that the initial change is an abrupt rise in the surface pressure; he called this a pressure jump. The pressure jump is followed by a quick change in wind direction (windshift) within 1 min. The "temperature break," defined as the beginning of a rapid temperature drop, follows the windshift by more than 2 min. The peak wind gust, rain onset, and pressure maximum successively follow the temperature break.

The surface changes accompanying the forward edge of the 31 May 1969 gust front at 2337:30 CST are shown schematically in Fig. 3. These "change" lines were extracted from analyses of the surface network fields. (Details of these fields will be discussed below.)

Fig. 3 depicts a complex structure. The first change is a pressure jump (PJ); a wind shift (WS) follows within 2 km. (For the remainder of this paper we will consider these change lines to coincide.) Eight kilometers northwest of the windshift (on the average) is a strong surge in wind speed called the gust surge (GS). (The term gust surge is adopted to differentiate the surge in wind speed from the combined changes in wind, temperature, and pressure that define the forward edge of the gust frontal air mass). Immediately following the gust surge is the temperature break line. The temperature break was accompanied by a pressure surge; this pressure surge added further to the pressure jump that had already occurred.

When the major surface changes at the leading edge of the squall line are considered together, we find good agreement with Tepper's model. Note that the order of the changes was pressure jump, windshift, gust surge, temperature break, and peak wind gust.

However, the picture is complicated by a double surge in surface pressure. Indeed, as we shall see later, the pressure curves at the network stations temporarily leveled off between the two surges. Note further, the temperature break and intense gust accompanied only the second of these pressure surges.

In later sub-sections we demonstrate that the second group of changes in Fig. 3 represents the gust front, i.e., the leading edge of the cold air outflow from the heavy-rain echoes. We will present evidence to show that the first pressure-wind change was not a direct reflection of the outflow; rather, it was associated with a separate mechanism. In the next two sub-sections we examine the structural details of the analyzed fields; the windshift-pressure jump and the gust front are discussed separately. After that we'll look to see if there was any connection between them.

1) WINDSHIFT-PRESSURE JUMP

The windshift is clearly evident in the wind analysis from the ground to 444 m (Fig. 4). It is marked and labeled "a" in all wind analyses except the gustiness. At the ground the wind changed from southerly to westerly over a span of 3 km (Fig. 4a). This isogon gradient gradually slacked off with height as seen in Fig. 4b. [The windshift is best depicted in the streamline patterns (Figs. 4c and 4d)]. Accompanying the wind direction shift was a minimum in wind speed (Figs. 4e and 4f) and gustiness (Figs. 4g and 4h). In all of these figures the windshift is seen to slope to the northwest with height; this slope is about 1 to 10.

The surface isogon and streamline fields (Figs. 4a and 4c) suggest that the flow near the windshift was fairly uniform in the y-direction near the frontal zone. The surface divergence field shown in Fig. 4c gives a good assessment of this apparent uniformity. This divergence field was computed on a rectangular grid with a mesh length of 5 km. Note that the divergence pattern is uniform along the windshift (WS) and gust surge (GS) zone.

We evaluated the ratio $(\partial u/\partial x)/(\partial v/\partial y)$ over the network to assess the validity of the streamfunction field in the x–z plane. In the region of section line $X\ Y$ in Fig. 4c this ratio was greater than 10 from point d southeastward. Northwest of point d the small scale variability decreases the ratio toward a value of 1. Returning to the windshift region, the isogon and isotach patterns above the ground in Fig. 4c and 4d are similar to those at the ground except for a phase lag.

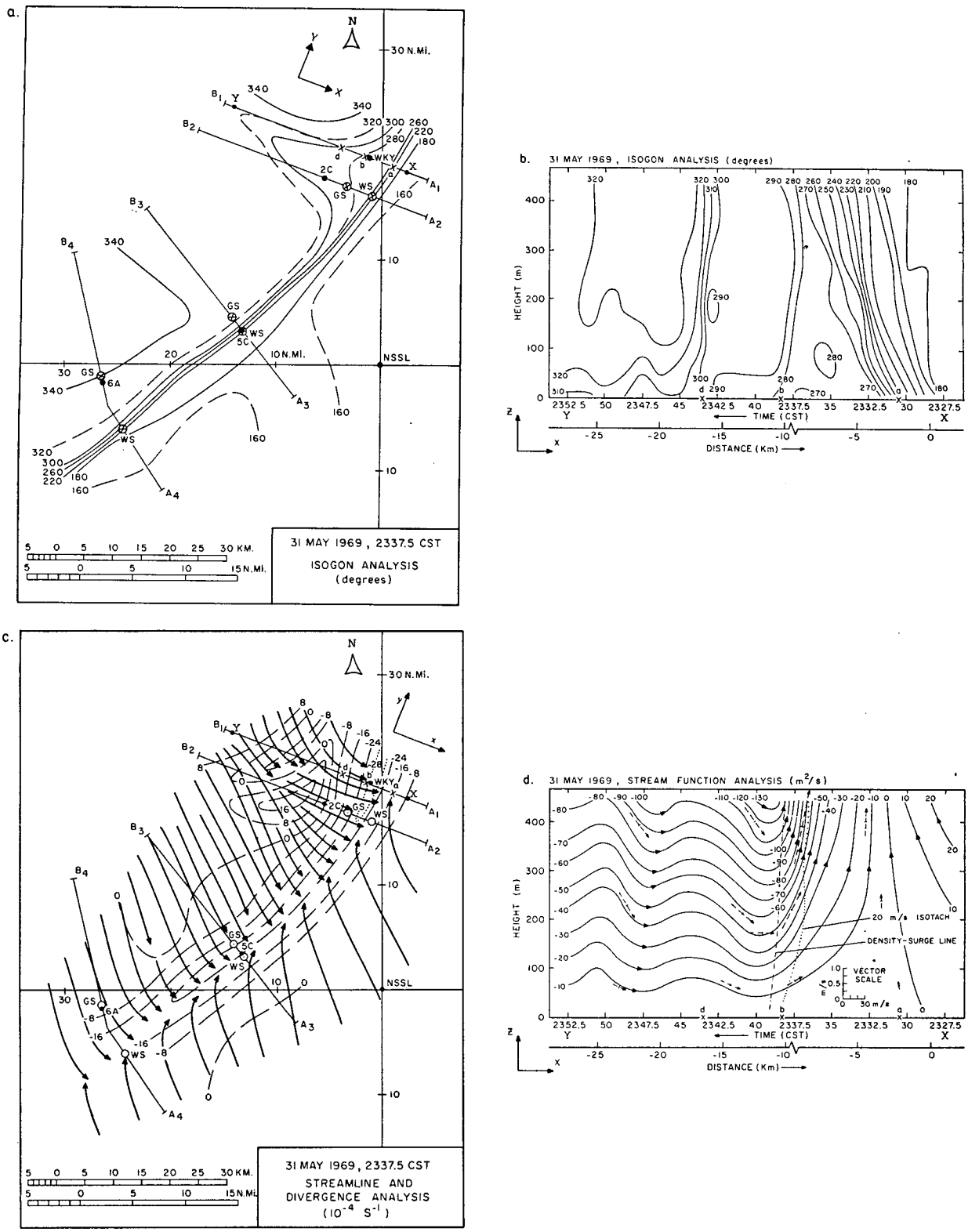

FIG. 4. (a–d). Network and tower wind analyses. Lines A_1B_1, A_2B_2, etc., superposed on all network fields represent section lines of the spatial sections shown in Fig. 5. The stations whose strip chart records were used in the construction of these sections are identified (see Fig. 2). In all surface fields, intersections of the windshift and the gust surge with the section lines are denoted WS and GS. Other features common to both the spatial sections in Fig. 5 and the network patterns are marked and labeled as shown. The lateral boundaries of the x–z plane analyses are denoted X and Y. The section line XY representing this plane is superposed upon line A_1B_1 in all surface network fields. Structural elements found both in the x–z plane fields and in the network fields are marked and labeled with lower case letters as shown. See text for further elaboration.

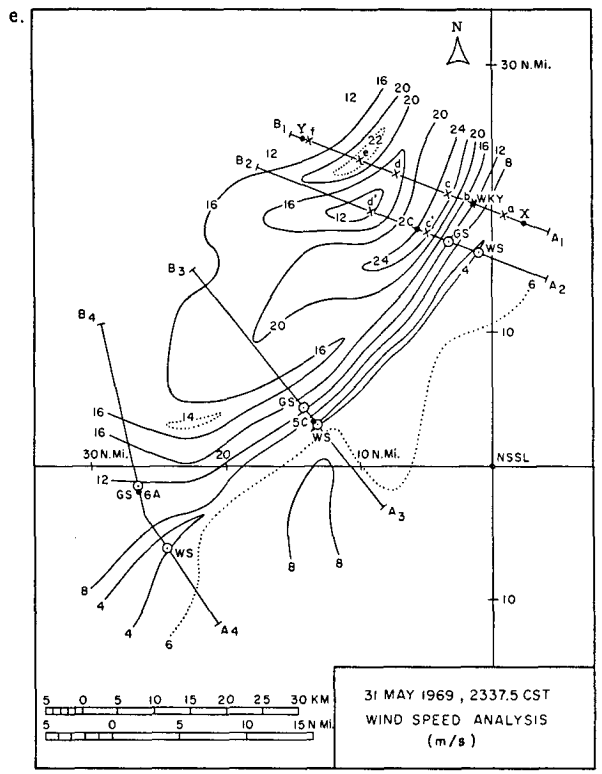

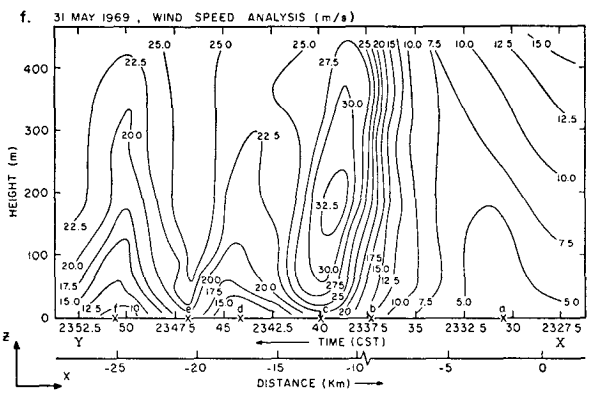

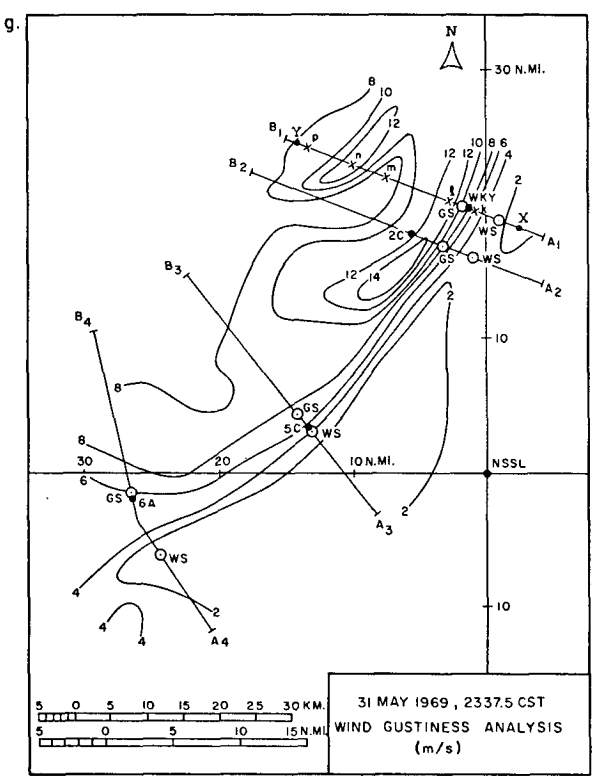

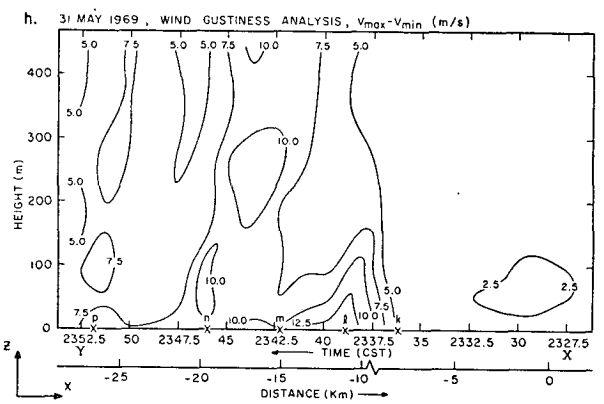

FIG. 4 (e–h). See Fig. 4 (a–d).

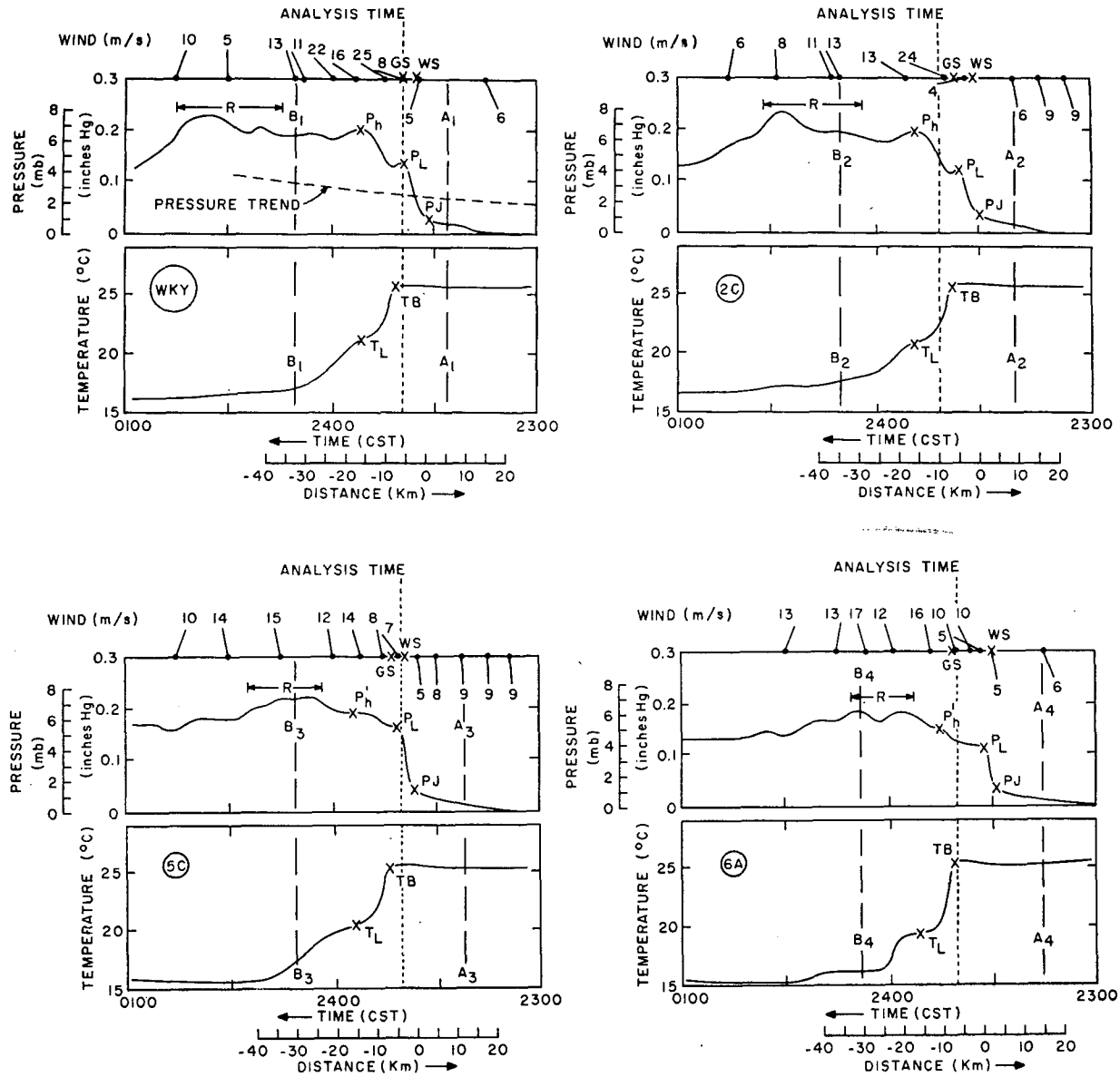

FIG. 5. Time-to-space scale sections of surface wind, pressure, and temperature normal to the leading edge of the gust frontal air mass at network stations WKY, 2C, 5C, and 6A. The long-dashed vertical lines labeled A_1 and B_1 at WKY, A_2 and B_2 at 2C, etc., denote the end points of the corresponding section lines A_1B_1, A_2B_2, etc., in the network fields. The short-dashed vertical line labeled "analysis time" denotes the time of the surface network analysis (2337:30 CST). Significant points along each curve are marked and labeled; these points are located in the appropriate network fields. In all sections "R" stands for heavy rain.

Therefore, it is reasonable to assume that $(\partial u/\partial x)/(\partial v/\partial y)$ remains much greater than 1 up to 444 m. This implies that the streamline field in Fig. 4d gives a good approximation of the actual flow in the x–y plane in the region around the WS and GS. (Upstream of, say, point d only the broad scale subsidence is considered to adequately approximate the true flow.)

Flow vectors computed from the streamfunction field (Fig. 4d) quantify the systematic upward motion field through the windshift. The vector scale in the inset shows that inserted vectors near the 400-m level depict upward motion of about 1 m sec^{-1}.

Across the surface network the wind change associated with the windshift is easily compared with corresponding changes in temperature and pressure in Fig. 5. One can see that the temperature remained steady while the pressure jump actually preceded the windshift. Indeed, the temperature analysis (Fig. 6a and 6b) showed the thermal pattern to be unchanging, not only at the ground, but also throughout the first 444 m. The wet-bulb temperature patterns (not shown) were similarly steady in this region.

Figs. 5 and 7 show that the pressure change through the windshift was uniformly intense across the network.

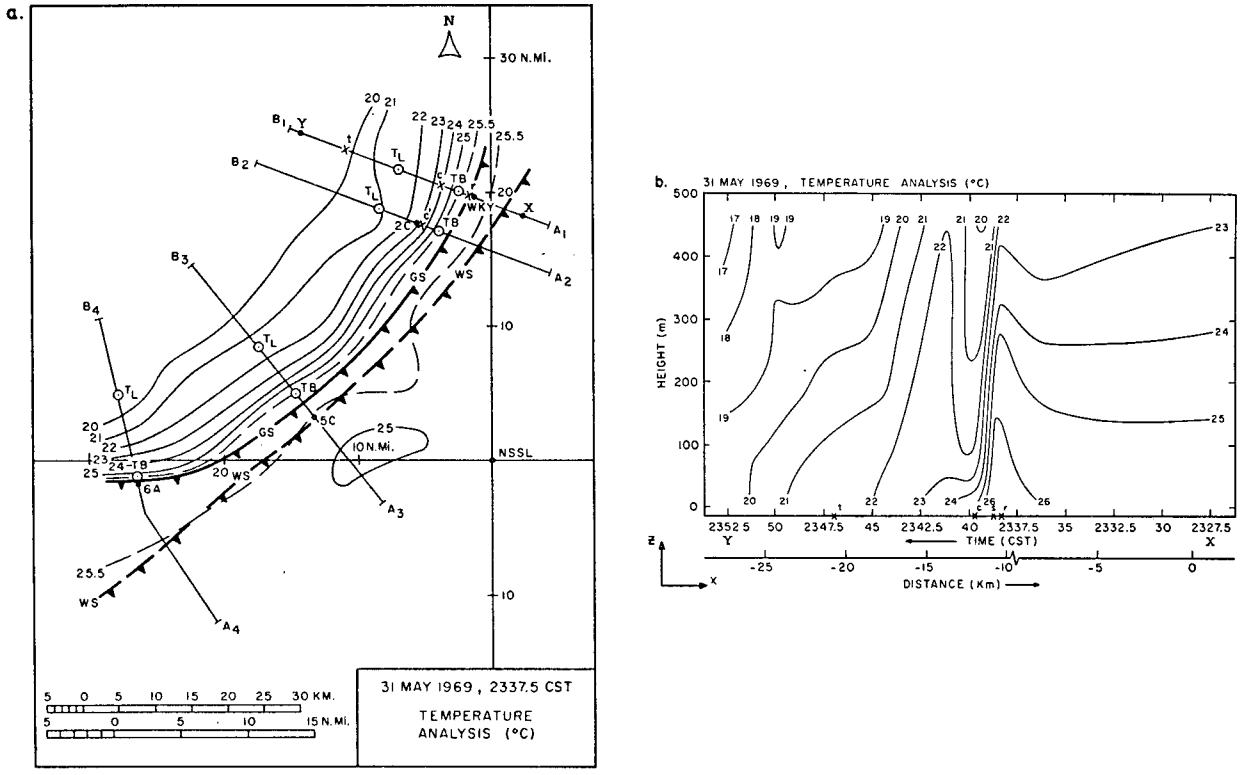

FIG. 6. Network and tower temperature analysis. Significant points along the section lines in (a) are denoted as discussed earlier (see Fig. 5).

The network average of the total pressure rise was 3.5 mb; the corresponding horizontal gradient was 0.6 mb km^{-1}. (Recall that the pressure field in Fig. 7 represents the mesoscale deviations from the large-scale trend. An example of this pressure trend is shown for station WKY in Fig. 5.)

2) GUST FRONT

The most prominent characteristic of the gust front was the initial surge in wind speed, i.e., the gust surge. This surge is best shown in Figs. 4e and 4f. The horizontal velocity divergence within the surge (where the $\partial u/\partial x$ term is grossly dominant) is as high as -30×10^{-4} sec^{-1} at the surface near WKY (Fig. 4c). However, when the grid spacing used to compute the divergence field in Fig. 4c is reduced from 5 km to 2.5 km near the frontal zone, the convergence was found to be an order of magnitude greater. Proceeding upward from the ground in Fig. 4f the horizontal gradient of wind speed $\partial u/\partial x$ increases with height to a maximum of -1.2×10^{-2} sec^{-1} near the 300-m level. This is consistent with convergence values obtained above a strong surface cold front by Browning and Harrold (1970).

Note that the wind speed surge sloped markedly in the forward direction with increasing height (Fig. 4f); this surge line rises only 150 m km^{-1} in the positive x-direction. This retardation near the ground is probably due to frictional drag.

A large area of maximum wind speed was found at the "crest" of the initial surge (Figs. 4e and 4f). Note in Fig. 4f that the maximum speed core, where values reached 35 m sec^{-1}, was only 200 m above the ground. The vertical wind shear in the first 50 m directly below this maximum was 160 m sec^{-1} km^{-1}. Appearing about 10 km upstream of the initial strong gust was a second wind surge labeled d in Fig. 4f. However, this secondary gust was relatively weak and, as seen in Fig. 4e, covered a small area. Therefore, we do not regard it as a significant feature in the overall circulation of the gust frontal air mass.

Although the gust front of 31 May had wind speeds more than twice as large as the Florida outflows studied by Goldman and Sloss, common characteristics in the initial gust are found in the isotach patterns. The surface retardation of the initial wind surge, the low-level maximum in speed near the leading edge of the outflow, and the large vertical shears near the ground were exhibited in both analyses. Interestingly, the vertical shears observed in the Florida cases are just as strong as found here even though the speeds are less.

The streamfunction pattern depicted a systematic vertical motion field within the gust frontal air mass (Fig. 4d). The strong upward flow seen at 2337:30 CST

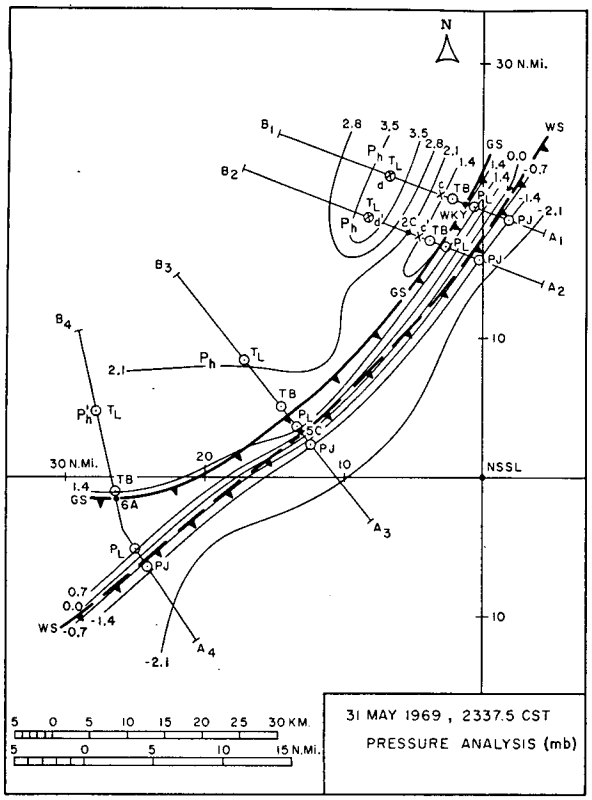

FIG. 7. Surface pressure analysis. This pressure analysis depicts mesoscale pressure deviations about the large scale trend. An example of the pressure trend is shown in Fig. 5 for WKY. For convenience in superposing features from other fields, significant points in the wind and temperature fields are also inserted on the section lines.

coincides with the initial surge (point *b* in Figs. 4d and 4f). At 400 m above the ground the upward velocity is 2.5 m sec^{-1}. (Smoothing over about 2 km horizontally and 100 m vertically is inherent in all vertical velocities obtained from Fig. 4d.) The downward component, coinciding with the rear side of the maximum speed core in Fig. 4f, was 0.8 m sec^{-1} at the same level. Upstream, the broadly subsiding flow averaged 0.15 m sec^{-1}.

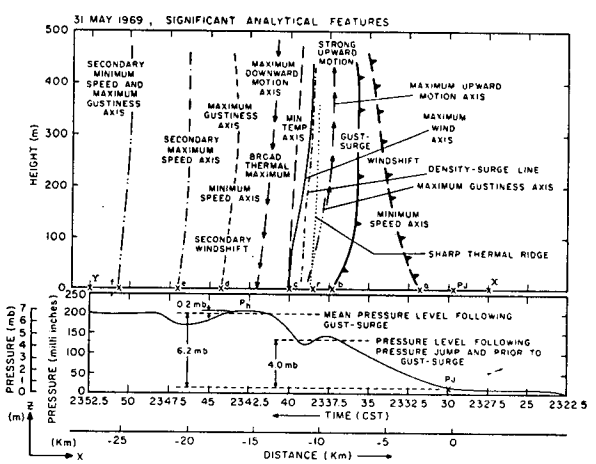

FIG. 8. Schematic of wind and thermal features composited from tower fields (upper). Pressure variation at the base of the tower (lower). This curve is the same as the WKY pressure curve in Fig. 5.

At the surface, areas of high wind gustiness coincided with areas of strong winds. In Fig. 4h the points of maximum surface gustiness, l and n, lie just ahead of the maximum speed points, c and e, in Fig. 4f. Above about 150 m a reverse tendency is seen on comparing Fig. 4h with Fig. 4f. Overall, high gustiness is seen beneath the forward sloping initial gust and all along the vertical column just behind the initial gust.

Some interesting features in the thermal field of the gust frontal air mass are found in Figs. 6a and 6b. Note i) the narrow thermal ridge (point r) just preceding the temperature break. Fig. 6a and Fig. 5 show that this ridge did not extend to the ground. ii) The horizontal temperature gradient defining the forward edge of the cold air was intense from the ground to 444 m. Averaged vertically through this layer, the gradient was 4C km^{-1}. iii) The cold-air boundary sloped forward with height at angle of about 1 (vertically) to 3 (horizontally). Therefore, the cold air overlies the warm air above point s in Fig. 6b, resulting in a superadiabatic temperature lapse rate in the air column. iv) A thermal ridge was found just upstream of the cold-air surge (around 2342 CST in Fig. 6b). Note how this ridge interrupts the gradual temperature decrease proceeding upstream from sharp temperature drop at the cold-air front. At the surface this feature appears as a zone where the sharp temperature fall temporarily levels off (point T_L in Figs. 5 and 6a) and then resumes as a more gradual temperature decrease. Fig. 4d shows that the air was sinking in this same region.

The surface pressure pattern (Fig. 7) shows that the pressure surge accompanying the gust front was greatest in the northern part of the network, i.e., around WKY. (In fact the surface wind pattern at station 2C was so similar to that at WKY that we translated some of the features indicated by lower case letters at WKY to section line A_2B_2 in Fig. 7.) The pressure peak, believed to be due only to the presence of the cold-air outflow, is labeled P_h in Figs. 5 and 7. The pressure rise that followed the gust surge and formed this pressure peak totalled 2.1 mb at both WKY and 2C; at 5C and 6A the corresponding value was only 0.7 mb.

Figs. 5 and 7 pose two other interesting features. One is that the P_h's occupy the same positions as the T_L's. The other, shown most clearly at stations WKY and 2C in Fig. 5, is that upsteram of the P_h's the pressure was practically steady up to the position of the heavy rain regions (denoted R). These features will have a profound impact upon the inferred shape of the upper surface of the cold air discussed in a later subsection.

For convenient reference in later discussions the

important wind and thermal features of the vertical cross sections are combined schematically in Fig. 8. The WKY pressure trace, transformed to the same scale as the schematic, is shown also.

Recall that our principal objective in this study was to examine the *complete* three-dimensional structure of the gust front. Of course, the lack of measurements inside the cold outflow above 444 m blocked structural analysis to greater heights. However, we could infer the depth of the cold air by extrapolating the temperature profile upward to some height such that the computed hydrostatic pressure increment at the ground matches the observed surface pressure rise accompanying the gust front. We could also estimate the flow pattern inside the boundaries of the cold air and outside as well by qualitatively applying the equation of continuity. But, before either of these tasks could proceed, it was necessary to resolve the question of possible physical-dynamical coupling between the observed windshift-pressure jump and the gust front. That is, was the leading pressure surge a reflection of the overlying cold air associated with the outflow (e.g., see Fig. 8) or was this pressure surge due to some mechanism relatively independent of the gust front? An answer to this question is needed in order to know the pressure rise directly attributed to the cold air.

b. *Relationship of windshift-pressure jump to the gust front*

Consider several hypothetical cases in which the windshift is physically coupled with the gust front. Fujita (1960) constructed a model showing the cold outflow pushing backward the previously advancing warm air, creating a low-level "back-current front" (Fig. 9). The return current ahead of the cold air could explain the windshift. However, the model does not explain the large pressure jump accompanying the 31 May windshift. As another theory one might consider the windshift as the remnant of a previously well-defined cold surge, subsequently diffused by mixing with warm air. This situation does not explain either the sharp pressure jump or the lack of any temperature change accompanying the windshift. Perhaps the most obvious explanation of the pressure jump ahead of the cold air is that the cold-air front above 444 m was located ahead of the front at the ground as also seen in Fujita's model (Fig. 9). However, to produce the observed pressure rises up to 3–4 mb a layer of cold air about 2 km thick would be required. And this layer must have moved 5 to 10 km ahead of the surface cold front to explain the observed conditions (Figs. 5 and 7). It is highly unlikely the convectively unstable condition that would exist below the upper front could be maintained over the time period that it took for the gust front to pass over the surface network, i.e., about 45 min.

In a more detailed account of this study (Charba, 1972) we demonstrated quantitative evidence which supports a theory that the windshift-pressure jump was associated with a gravitational wave (see Tepper, 1950, 1955). This wave could have propagated on the thermal inversion seen at 2.3 km in Fig. 10. Obviously, such a gravitational wave and a thunderstorm outflow

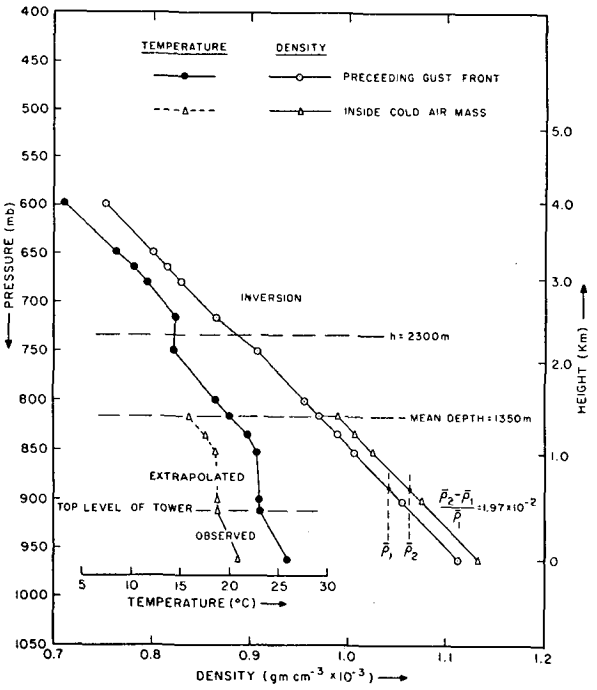

FIG. 10. Density and temperature (inset) versus height curves at WKY before and after the gust front passed (2300 CST and 2345 CST, respectively). The temperature profile in the cold air above 444 m was inferred by extrapolating the temperature curve upward from below, parallel to the ambient temperature curve. The quantities ρ_1 and ρ_2 are mean densities in the warm and cold air below 1350 m.

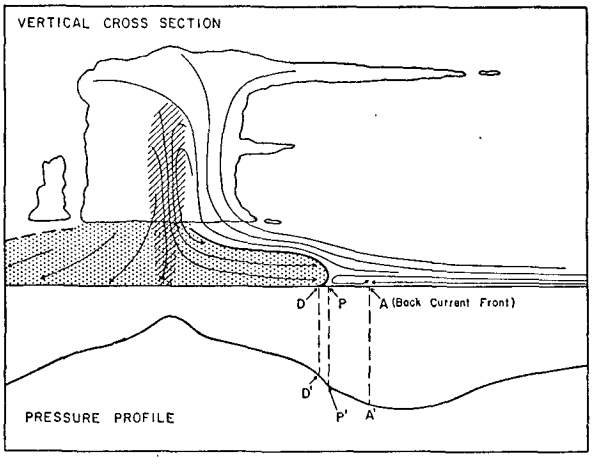

FIG. 9. Schematic model of the low-level air flow inside and outside of thunderstorm outflows (from Fujita, 1960). Fujita drew this model on the basis of his analysis of surface and upper air mesonetwork data from the Thunderstorm Project. In particular, please note the "back current front."

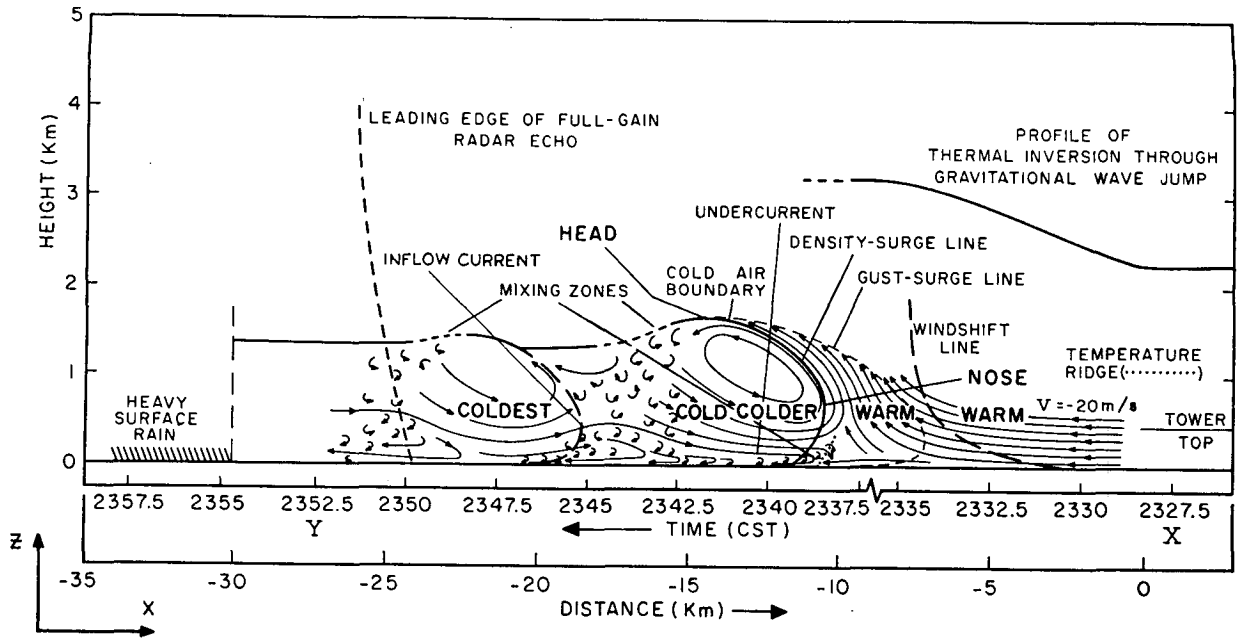

FIG. 11. Schematic structure of the windshift-pressure jump and gust front associated with the 31 May 1969 squall line. Compare the gust front structure with the structure of a laboratory simulation model of a gravity current (Fig. 13b). See text for discussion.

are different atmospheric phenomena and therefore separate in all respects. A schematic of the postulated wave on the thermal inversion, juxtaposed next to the gust front, is shown in Fig. 11.

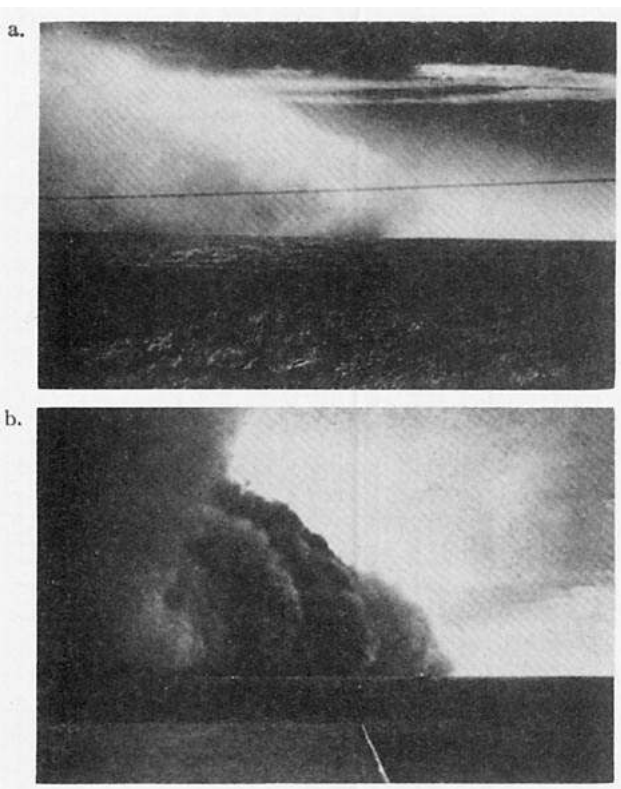

FIG. 12. Photographs of advancing fronts of dust-laden cold air masses. (a) Cold front in Kansas. (Permission for reproduction granted by Annual Review of Fluid Jechanics; see Yih, 1969.) (b) "Downdraft haboob" in Sudan (courtesy of Simpson, 1969).

The arguments just presented and the facts given in our detailed report are not really sufficient to conclude that the mechanism of the windshift-pressure jump was the postulated gravity wave; however, when all the above evidence is combined we feel it is reasonable to conclude that the wind and pressure disturbance, leading the gust front was not a physical reflection of the cold air outflow. This is the only conclusion really relevant to the investigation of the gust frontal air mass above 444 m.

1) COLD-AIR DEPTH

The depth of the cold air mass was deduced by extrapolating the temperature profile below 444 m upwards and applying the hydrostatic equation. The temperature curve was extrapolated as illustrated in Fig. 10. The temperature curve preceding the gust front is based upon the Tinker Air Force Base rawinsonde (located about 5 n mi southeast of WKY) at 1800 CST, 31 May; the sounding was updated in the lowest 444 m by inserting the WKY tower temperatures and surface pressure measured just before the gust front arrived. The temperature curve below 444 m in Fig. 10 represents the mean temperature profile inside the cold air upstream of the initial surge in Fig. 6b; this profile is extrapolated above 444 m in Fig. 10 as shown.

The depth of the cold air was determined by repeated integrations of the hydrostatic equation for successive estimates of the depth required to account for the surface pressure surge accompanying the cold air.

Using the mean temperature curve in Fig. 10 and the mean pressure rise at WKY of +2.2 mb (see Fig. 8), the computed depth is 1350 m.

The detailed shape of the upper surface of the cold air was determined by applying the above procedure along many vertical columns of the x–z plane section using temperatures in Fig. 6b and the pressure curve in Fig. 8. The results are shown in Fig. 11. (We shall reserve discussion of the deduced geometry of the upper cold air surface for the next sub-section.)

2) Circulation field

The air-motion field near the leading edge of the cold air mass was deduced by the following procedure: i) The analyzed field of wind components in the x–z plane below 444 m in Fig. 4d was projected upward to 1350 m in both the warm and cold air, away from the frontal zone. In these regions the assumption of uniformity of the air flow in the vertical is most reasonable. ii) We assumed that flow across the interface separating the air masses did not occur above 750 m, i.e., along the upper surface of the nose shown in Fig. 11. Our reasoning was that warm-cold air mixing in this region would be suppressed because of the high static stability. And, iii) the mass continuity equation for incompressible flow was applied, qualitatively, to the analyzed and inferred flow patterns in the x–z plane. This procedure gave a crude estimate of the basic circulation pattern near the leading edge of the gust front above the top of the tower. The validity of this hand-craft approach rests upon the earlier finding that $\partial u/\partial x \gg \partial v/\partial y$ in the vicinity of the leading edge of the gust front. (The circulation field thus deduced, shown in Fig. 11, is discussed in the following sub-section.)

d. Composite structure of the gust front

A schematic drawing of the flow and thermal structure of the 31 May 1969 gust front is shown in Fig. 11. From the ground to 444 m, the structure is composited entirely from the analysis; at greater heights it was deduced as just described.

The geometry of the cold-air surface contains several features that are worth examining in some detail (Fig. 11). At the leading edge note that the cold air projects into the warm air with a blunt shaped "nose."[3] The foremost projection of the nose is located 750 m above the ground and 1.3 km ahead of the cold-air boundary at the ground.

Studies of the surface geometry of dense clouds of dust which characterize haboobs have been conducted by Sutton (1925), Farquharson (1937), Freeman (1952), Lawson (1971) and Idso *et al.* (1972). In most cases a projecting nose similar to that found in the 31 May gust front was found. Typical examples are reproduced in Fig. 12.

[3] Some of the prominent features of the gust front are named after analogous properties of laboratory-produced gravity currents. Gravity currents and similarities between gravity currents and this gust front will be discussed in the next section.

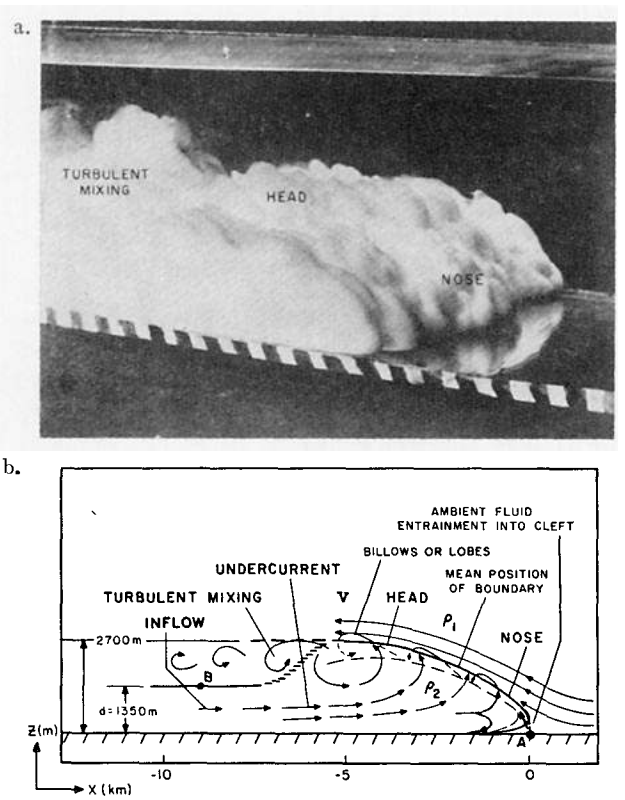

FIG. 13. (a) A gravity current (also called density current) simulated in a laboratory experiment (reproduced from Simpson, 1969). The white mass is a saline solution, flowing to the right along the bottom of a trough filled with pure water (compare with Fig. 12). (b) Schematic (laboratory) gravity current mode, (constructed from the work of Keulegan, 1958; Middleton, 1966; and Simpson, 1969; 1972). The vertical and horizontal dimensions of the model are scaled to the dimensions of the gust front.

In studies of sea-breeze fronts and in other studies of gust fronts, descriptions of the structure of the forward edge of the cold air mass are rather conflicting. From visual observations of hazy sea-breeze air masses, Simpson (1969) observed noses similar to those shown in Fig. 11. On the other hand, Koschmeider's (1932, 1941) analysis suggests that the forward cold-air profile changes with time and in space in individual sea-breeze fronts. Similarly, Colmer's (1971) examination of 13 gust front cases disclosed that the vertical profile of the horizontal wind-shear line in the layer 0–444 m slopes both forward and backward from case to case. Goldman and Sloss's (1969) high resolution thermal analysis of a Florida thunderstorm gust front showed a forward slope similar to that found in this study. These conflicting findings may be interpreted to mean that (in at least some cases) the overhanging cold air periodically collapses into the warm air beneath it. With this in mind, it is speculated that the narrow thermal ridge beneath the overhanging nose may be a

result of compressional warming below the gradually collapsing under-side of the nose (Fig. 11).

In Fig. 11 two features highlight the general shape of upper surface of the cold air mass. First is the vertical bulge near the front of the air mass, called the "head." The height to the top of the head is 1700 m. Second is the relative flatness and shallowness of the upper surface upstream of the head; here the cold-air depth was only 1350 m.

From their analyses of cold fronts and sea-breeze fronts, Berson (1958), Clarke (1961), and Browning and Harrold (1970) have given a broad view of the geometry of the forward portion of these air masses. In most cases vertical bulges in the cold air were indicated near the leading edge; upstream, the upper boundary was quasi-horizontal for sometimes tens of kilometers before resuming an upward slope (particularly, in the case of cold fronts). However, it is crude to draw a parallel between these vertical bulges and the gust front head because the data density involved in the above studies was insufficient to resolve air-mass structural elements several kilometers in size. In contrast, the near-constant depth region, some distance upstream of the respective air mass fronts, clearly seems to be similar.

Ball's (1960) theoretical treatment of the cold fronts predicts that the upper surface of the cold air mass tends toward the horizontal in regions where frictional stress is large. Clarke's (1961) investigation suggests that a balance between frictional stress and horizontal pressure gradient extends up to about 30 km upstream of surface cold fronts and sea-breeze fronts. Thus, on the basis of Ball's and Clarke's findings it can be reasoned that the head and uniform depth features which characterized the gust front were caused by frictional stress.

The air flow pattern associated with the gust front (Fig. 11) was constructed relative to a coordinate system moving toward the right of the page at the speed of the gust front, 20 m sec^{-1}. (This is the translation speed of the gust front relative to the mean motion of the ambient warm air.) Viewed in this frame of reference it is plain to see that strong upward motion occurred when the warm air was lifted by the blunt nose. Earlier we mentioned that the computed upward flow component of 2.5 m sec^{-1} at 400 m is a conservative estimate of more localized values. In addition, the intense velocity convergence of 10^{-2} sec^{-1} persisted up to the tower summit with no evidence that it would be abruptly relaxed at increasing heights. From application of mass continuity as described earlier we obtained an estimate of upward motion of 7.5 m sec^{-1} at the 800-m level, just ahead of the cold-air boundary. This is consistent with Doppler radar measurements of vertical motion above a surface cold front reported by Browning and Harrold (1970).

The most prominent characteristic of the flow pattern inside the outflow air mass is the strong forward current at low-levels beneath the head (Fig. 11). This current reflects the maximum wind speed cell in Fig. 4f. Since this high speed current is centered only a small distance above the ground and beneath the head, it is called an undercurrent. Relative to the coordinate system adopted in Fig. 11 the forward speed at the core is 14 m sec^{-1}.

In considerations taken up in the next section we shall often refer to the gust frontal air mass as a high-density air current. Now, recalling earlier discussion of the thermal structure, we emphasized the sharp thermal gradient marking the forward boundary of the cold air. Therefore, we now choose to call this forward boundary the "density surge" line (Fig. 11). For convenient reference, this line has also been inserted in Figs. 4d and 8.

In Fig. 11 note that streamlines cross the density-surge line in the region where the undercurrent impinges upon the cold-air front. Analytical support for this feature can be demonstrated from Fig. 4d. Viewing the flow in this figure with respect to the translating coordinate axis adopted in Fig. 11, the horizontal component of motion normal to the 20 m sec^{-1} isotach is zero. Recall from Fig. 4f that the forward speed of the current increases sharply to the left of the 20 m sec^{-1} isotach; thus, a component of flow transverse to the density-surge line is implied. Mixing of warm and cold air within the density-surge zone would be required to explain the warming of the air as it flows through this region. The large gustiness below 200 m within the horizontal strip between points k and m in Fig. 4h corroborates this reasoning. The strong vertical wind shear and slightly superadiabatic lapse rate which characterized this air volume provide a favorable environment for mixing. Eddies associated with the mixing process are shown in Fig. 11 by short curled vectors. This turbulent region in the frontal zone is consistent with Martin's (1973) observations of the fine scale turbulence structure of cold frontal zones.

The flow pattern in Fig. 11 at low levels, beneath the head and in the nose, is consistent with both measurements of dust content and the visual motion of dust-cloud lobes at the leading edge of haboobs (see Lawson, 1971, and Idso *et al.*, 1972). Furthermore, it makes plausible a mechanism for dust cloud generation consistent with observations. Dust, entrained into the cold air mass where surface winds are usually strongest, is transported to the noise where it is mixed with warm air; there it is carried up by a strong upward current to the great heights seen in photographs (see Fig. 12). This motion field is also consistent with observations of "roll cloud" formations along cold-frontal zones[4] (also see Livingston, 1972).

The flow shown along the back side of the head in Fig. 11 reflects the analysis below 444 m and provides

[4] Prof. Y. Sasaki (Department of Meteorology, University of Oklahoma) has made a time-lapse movie of such a cloud formation which appeared in Norman, Okla., during the spring of 1972.

a basis for hypothesis of an important air-entrainment mechanism. This down-motion side of the closed circulation cell accounts for both the downward motion region shown in Fig. 4d and the coincident thermal maximum shown in Fig. 6b. High wind gustiness (see Fig. 4h) and large fluctuations in temperature records (not shown) characterized this air column. (These temperature oscillations had amplitudes up to 0.4C.) Taking into account the large gustiness and the downward motion, it is postulated that turbulent mixing occurred in the wake of the head crest, resulting in entrainment of environmental air. This turbulent air mixture is then slowly transported downward and may be partly entrained into the undercurrent (see Martin, 1973).

In Fig. 11 note the weakly descending air current flowing into the high speed undercurrent. This current originates far upstream in the rain area of the squall line; the speed relative to the head is 4 m sec^{-1}. This influx of cold air apparently maintained the sharp thermal gradient at the front of the advancing air mass, in opposition to the diluting effect of warm-air entrainment. This flow feature is also consistent with a schematic flow model of thunderstorm outflows proposed by Byers and Braham (1949).

The general internal flow pattern of the high density current in Fig. 11 resembles analytical streamline fields of cold fronts and sea-breeze fronts in Australia reported by Berson (1958) and Clarke (1961) and of cold fronts in the British Isles studied by Browning and Harrold (1970). The major difference is that the 31 May gust front had a stronger and better organized circulation field inside the head; this is coupled with a stronger initial gust. There is also a striking resemblence in structure between the internal flow of the gust front and Prandtl's (1952, pp. 369–370) simplified flow model of a cold front.

5. Application of gravity current model to gust front

A gravity current (also called density current) is a mass of high density fluid, flowing along the horizontal bottom and displacing an ambient fluid of lesser density. The current is driven by a horizontal pressure gradient acting across the lateral interface separating the two fluids. The pressure gradient exists because the hydrostatic pressure inside the dense fluid is greater than it is in the less dense fluid. Under steady conditions, the pressure gradient force is balanced by dynamic pressure acting against the front of the heavy fluid mass and shear stress at the boundaries. Among commonly known examples of gravity currents occurring in nature is one in which a mass of saline water intrudes into a fresh water estuary (saline current) or when a mass of muddy water displaces clear water along the bottom of a reservoir ("turbidity current").

Previous studies have shown that some types of atmospheric cold air masses exhibit some properties of gravity currents. Such evidence has been found associated with the leading edge of cold fronts by Berson (1958), with sea-breeze fronts by Simpson (1969), and with "downdraft" haboobs by Simpson (1969) and Idso *et al.* (1972). In the following discussion, we attempt to demonstrate that the 31 May gust front exhibited both structural and dynamic characteristics that distinguish gravity currents.

a. Structure

Much of what is presently known of the structure and horizontal propagation of gravity currents has been learned from observations and measurements of laboratory models (Keulegan, 1958; Middleton, 1966; and Simpson, 1969, 1972). In most experiments with such models, relatively dense liquid solutions are used to produce gravity currents in long flumes filled with a less dense fluid. A gravity current is formed when a lateral partition confining the denser fluid is removed and the heavy mass surges horizontally along the bottom of the flume. A photograph of such a gravity current is shown in Fig. 13a; the white mass is a saline solution of specific gravity 1.01. It is propagating to the right along the bottom of a trough filled with pure water. A comparison of Fig. 13a with Fig. 12 reveals noteworthy similarity between the gravity current and atmospheric cold-air surges.

The structure and circulation of laboratory models of gravity currents are shown in Fig. 13b. This schematic was composited from documented studies wherein the associated density ratios (defined by $(\rho_2-\rho_1)/\rho_1$, where ρ_2 refers to the density of the gravity current) are typical of atmospheric cold-air surges. The overall shape is based upon extensive work of Keulegan (1958); however, the nose overhang has been examined just recently by Simpson (1972). The vertical and horizontal dimensions shown in Fig. 13b were obtained by multiplying Keulegan's nondimensional values of mean upstream depth and head length and depth by the corresponding dimensions exhibited by the 31 May gust front. The circulation field is patterned after the findings of Middleton (1966) and Simpson (1969, 1972). Simpson found that the region beneath the nose is convective, i.e., trapped parcels of the lighter fluid rise while the onrushing dense fluid sinks. Veins of the rising fluid form clefts in the nose; this gives the nose a lobed or billowed substructure and allows for further entrainment of environmental fluid. Under certain conditions the billows roll up as they proceed upward along the upper surface of the head and break up in the turbulent wake region (see Figs. 13a and 13b). Both Keulegan and Middleton noted copious dilution of the dense fluid in the wake, indicating entrainment of ambient fluid.

Comparing the respective structures of the 31 May gust front and the gravity current model (Figs. 11 and 13b), we can see significant similarity in the surface geometry, internal densimetric structure, and flow

TABLE 1. Application of gravity current theory.

Mean depth d(m)	Density ratio $(\bar{\rho}_2-\bar{\rho}_1)/\bar{\rho}_1$	Displacement speed of front (m sec^{-1}) Theoretical $1.414\,G^*$	Empirical $1.090\,G^*$	Observed V_{obs}	Froude number $k(=V_{obs}/G^*)$
1350	1.97×10^{-2}	22.7	17.5	20.0	1.250

$G^*=\sqrt{gd\frac{\bar{\rho}_2-\bar{\rho}_1}{\bar{\rho}_1}}$.

pattern. The general likeness of many features is obvious from these schematics, as identical labeling of analogous features provides for easy comparison; thus, further comment is unnecessary. However there are similarities and differences in detail that bear mention. One notable difference in geometry is in the head height; the gravity current head is 2700 m while its gust front counterpart was only 1700 m. Another difference is in the height of the nose above the ground: 750 m for the gust front versus 400 m for the gravity current. Even the fine-scale densimetric structure of the gust front (as implied by its thermal structure) is consistent with the densimetric structure of the fluid gravity currents. The relatively warm air in the upper regions of the wake may be a reflection of turbulent entrainment of environment air analogous to observations in gravity currents. However, in each of these counterparts, the influx of cold air (dense fluid) at low levels, originating from an upstream source region, apparently maintains the low temperature (high density) inside the head against this and other dissipating effects. Again, in each case, the ambient medium beneath the nose apparently finds itself trapped beneath the dense medium. As indicated in previous discussion of the gust frontal structure, warm-cold air mixing in this region is indicated. In studies of haboob fronts, Lawson (1971) inferred that volumes of warm air, equalling that in the lobes of cold air, are entrained into the curtain-like folds in the nose. Of course such quantitative inferences cannot be made from our data.

b) Dynamics

The forces that govern gravity-current motion are hydrostatic pressure, dynamic pressure, and friction. We have already mentioned Ball's (1960) finding that large frictional stress can have a significant effect on the shape of the cold-frontal surfaces. However, when friction is included in the equations of motion the mathematics become unmanageable; therefore, the usual practice has been to assume ideal fluid flow.

In one of the first attempts at theoretical analysis, von Kármán (1940) applied Bernoulli's equation for steady, ideal flow along the streamline separating the gravity current and the ambient fluid. Without going into mathematical details, this approach can be illustrated from Fig. 13b. Assume i) idealized gravity current flow, i.e., no frictional stress, and ii) that the pressure is hydrostatic along the interface separating the two fluids, except at point A where stagnation exists. A relationship is obtained for the displacement speed, V, of the gravity current given by

$$V=k\sqrt{gd\frac{\rho_2-\rho_1}{\rho_1}} \tag{2}$$

where ρ_2 and d is the density and mean depth of the gravity current, ρ_1 is the density of the ambient medium and g is the gravitational constant. Eq. (2), or slight variations of it, can also be obtained from several different approaches (see Benjamin, 1968, and Daly and Pracht, 1968).

Upon inspecting (2) it will be noted that k is the square root of the ratio of inertial to gravitational forces. Therefore, it is the square root of the internal Froude Number of the gravity current. The value of k yielded by the derivation of (2) is $\sqrt{2}$.

Keulegan (1958) and Middleton (1966) applied (2) to their laboratory models. For models having density ratios typical of atmospheric cold surges they obtained an empirical value of k of 1.09 as an average. Daly and Pracht (1968) developed a numerical model of gravity currents. Upon applying a relationship essentially the same as (2) to their model motion they got k values similar to Keulegan's and Middleton's.

It should be valid to apply (2) to the 31 May gust front since the condition $\partial u/\partial x \gg \partial v/\partial y$ is generally valid in the region of the analysis (Fig. 11). In the application of (2) we incorporated mean densities over the 0–1350 m layer in the warm and cold air (see Fig. 10). The resulting (theoretical) horizontal displacement speed and the observed speed of the gust front relative to the environment are shown in Table 1; the Froude number of the gust front is also included. The closeness of agreement between both the theoretical and observed speeds and in the respective Froude Numbers clearly suggests the dynamics of motion of the gust front is similar to the gravity-current model.

Combining the similarity in structure discussed in the previous sub-section with the apparent similarity in dynamics, overall agreement between the gravity current model and the 31 May gust frontal air mass is reasonably well demonstrated.

Of course, more cases need to be examined in order to test the general applicability of the gravity-current model to thunderstorm outflows. For valid tests the gust front cases selected for study should be similar in maturity, size, and strength to the one examined here. In fact the great likeness of 31 May cold-air outflow with the gravity current model may rest upon the observed conditions that, i) its forward speed was temporally steady, ii) its forward edge was far ahead of the heavy precipitation echoes, and iii) its general structure was spatially uniform and temporally steady.

6. Summary and conclusions

The wind and thermal structure of a strong squall line gust front has been synthesized from high spatial resolution analysis in three dimensions. Much tedious effort was invested to resolve wavelengths as small as 10 km.

The major structural features of the gust front were (see Fig. 11):

i) *Large wind and temperature gradients in the frontal zone.* The horizontal wind shear, averaged 2 km horizontally and 300 m vertically, was 8 m sec^{-1} km^{-1}. This large shear was reflected in the magnitude of the horizontal divergence of the wind; it was of the order of 10^{-2} sec^{-1}. In the same region, the vertically-averaged horizontal temperature gradient was 4C km^{-1}.

ii) *Distinctive geometry of the cold air surface.* In a vertical cross section (Fig. 11) the outflow air mass revealed a well-marked vertical bulge near its leading edge; this was called a head. The depth through the head was 1700 m. Upstream of the head the upper surface was quasi-horizontal and the depth was only 1350 m. Along the frontal zone, the cold-air front at the ground lagged the foremost extension of the cold air aloft by 1.3 km. This overhang of cold air is labeled "nose" in Fig. 11.

iii) *Systematic flow pattern inside the head.* The peak wind gust was found beneath the head only 175 m above the ground (Fig. 11). This high-speed "undercurrent" exceeded the forward speed of the gust front (20 m sec^{-1}) by 14 m sec^{-1}. The undercurrent was apparently fed by a slowly subsiding cold current originating 20 km upstream in the heavy rain cells of the squall line. Upward motion estimated at 5–10 m sec^{-1} occurred ahead of and within the nose of the cold air; weaker downward motion characterized the region to the rear of the head.

iv) *Evidence of warm air entrainment into the head.* We found evidence suggesting that turbulent cold-warm air mixing occurred within the wake of the head. Additional entrainment was evident beneath the nose where the warm air was apparently trapped beneath the overshooting cold air.

The presence of sharp thermal gradients along the frontal zone, coupled with evidence of entrainment of warm air into the head, leads us to suggest the upstream (inflowing) current noted in (iii) served to reinforce the cold air at the forward edge of the air mass. In addition, the unique structure of the temperature and wind fields described in (ii) and (iii) is likely due largely to surface friction.

We found that the shape and flow fields of fluid gravity currents produced in laboratory experiments are similar to corresponding structural components of the 31 May gust front (compare Fig. 11, and Fig. 13b). In general, the laboratory gravity current model has a more protruding head but its nose is more streamlined. We also found that the forward speed of the gust front agrees with empirical and dynamical relations describing gravity current motion (see Table 1). This evidence provides the basis of our belief that the 31 May gust front is well described by the gravity current model.

Acknowledgments. I express my sincere thanks to Prof. Yoshikazu Sasaki, University of Oklahoma, for guiding me in this research and for reviewing the manuscript. I also thank all NSSL personnel who helped collect the data. Special appreciation is extended to Drs. Edwin Kessler (NSSL Director) and Stanley L. Barnes (NSSL), Mr. R. Craig Goff (NSSL), and Prof. Rex L. Inman (OU) who contributed constructive criticism and suggestions on the investigation and on the manuscript. Drs. Celso Barrientos and Mikhail Alaka of the Techniques Development Laboratory gave further beneficial criticism on the manuscript. Jocelyn Boss and my wife, Ramona, did the typing.

This research was supported by NOAA Grant No. E22-43-706 through the Environmental Research Laboratories National Severe Storms Laboratory.

REFERENCES

Ball, F. K., 1960: A theory of fronts in relation to surface stress. *Quart. J. Roy. Meteor. Soc.*, **86**, 51–66.

Barclay, P. A., and K. E. Wilk, 1970: Severe thunderstorm radar echo motion and related weather events hazardous to aviation operations. ESSA Tech. Memo. ERLTM-NSSL, No. 46, 63 pp. (Reports in this series are available from the National Technical Information Service, Operations Division, Springfield, Va. 22151.

Barnes, S. L., J. H. Henderson, and R. J. Ketchum, 1971: Rawinsonde observation and processing techniques at the National Severe Storms Laboratory. NOAA Tech. Memo. ERLTM-NSSL, No. 53, 246 pp. (See above for availability of reports.)

Benjamin, T. B., 1968: Gravity currents and related phenomena. *J. Fluid Mech.*, **31**, Part 2, 209–248.

Berson, F. A., 1958: Some measurements of undercutting cold air. *Quart. J. Roy. Meteor. Soc.*, **84**, 1–16.

Browning, K. A., and T. W. Harrold, 1970: Air motion and precipitation growth at a cold front. *Quart. J. Roy. Meteor. Soc.*, **96**, 369–398.

Byers, H. R., and R. R. Braham, Jr., 1949: *The Thunderstorm.* U. S. Gov't. Printing Office, 287 pp.

Carter, J. K., 1970: The meteorological instrumented WKY-TV tower facility. NOAA Tech. Memo. ERLTM-NSSL, No. 50, 18 pp. (See above for availability of reports.)

Charba, J., and Y. Sasaki, 1971a: Structure and movement of the severe thunderstorms of 3 April 1964 as revealed from radar and surface meso-network data analysis. *J. Meteor. Soc. Japan*, **49**, 191–214.

——, 1971b: Gravity current model applied to analysis of squall-line gust front. Preprints of Seventh Conf. on Severe Local Storms, Am. Meteor. Soc., Boston, Mass., 277–283. (Unpublished).

Charba, J., 1972: Gravity current model applied to analysis of squall line gust front. NOAA Tech. Memo. ERLTM-NSSL, No. 61, 58 pp. (See above for availability of reports.)

Clarke, R. H., 1961: Mesostructure of dry cold fronts over featureless terrain. *J. Meteor.*, **18**, 715–735.

Colmer, M. G., 1971: On the character of thunderstorm gust fronts. Royal Aircraft Establishment, Bedford, England, 11 pp.

Daly, B. J., and W. E. Pracht, 1968: Numerical study of density current surges. *Phys. Fluids*, **11**, 15–30.

Farquharson, J. S., 1937: Haboobs and instability in Sudan. *Quart. J. Roy. Meteor. Soc.*, **63**, 393–414.

Freeman, M. H., 1952: Dust-storms of the Anglo-Egyptian Sudan. Meteorological Office, London, England, Report 2, No. 11, 20 pp.

Fujita, T., 1960: Mesometeorological study of pressure and wind fields beneath isolated radar echoes. Univ. of Chicago, Dept. of Meteor., Final Rep. to U. S. Wea. Bur., Contract No. Cwb 9762, pp. 1–5.

——, 1963: Analytical Mesometeorology: A Review. *Meteor. Monog.*, **5**, 77–125.

——, 1967: Detailed investigation of mesometeorological conditions of the squall line of August 6–7, 1966, which crossed the air route between Kansas City, Missouri and Omaha, Nebraska. Part III: Turbulence in relation to the squall line. Prepared for the British Aircraft Corp. Inc., Dept. of Geophysical Sciences, The Univ. of Chicago, Chicago, Ill., 27 pp.

Goldman, J. L., and P. W. Sloss, 1969: Structure of the leading edge of thunderstorm cold-air outflow. Preprints of the Sixth Conf. on Severe Local Storms, Am. Meteor. Soc., Boston, Mass., 71–74. (Unpublished).

Idso, S. B., R. S. Ingram, and J. M. Pritchard, 1972: An American haboob. *Bull. Amer. Meteor.*, **53**, 930–935.

Keulegan, G., 1958: The motion of saline fronts in still water. Nat. Bur. of Standards Rep., U. S. Dept. of Comm., Wash., D. C., 29 pp.

Koschmieder, H., 1932: Danziger seewind studien I. *Forch Met. Inst.*, **8**, 4 pp.

——, 1941: Danziger seewind studien II. *Forch Met. Inst.*, **10**, 39 pp.

Lawson, T. J., 1971: Haboob structure at Khartoum. *Weather*, **26**, 105–112.

Livingston, R. L., 1972: An unusual arcus cloud. *Mon. Wea. Rev.*, **100**, 817–818.

Martin, H. C., 1973: Some observations of the microstructure of dry cold fronts. *J. Appl. Meteor.*, **12**, 658–663.

Middleton, G. V., 1966: Experiments on density and turbitity currents. *Canadian J. Earth Sc.*, **3**, 523–546.

Prandtl, L., 1969: *Essentials of Fluid Dynamics with Applications to Hydraulics, Aeronautics, Meteorology, and Other Subjects.* Blackie and Son, Limited, London and Glascow, England, 452 pp.

Simpson, J. E., 1969: A comparison between laboratory and atmospheric density currents. *Quart. J. Roy. Meteor. Soc.*, **95**, 758–765.

——, 1972: Effects of the lower boundary on the head of a gravity current. *J. Fluid Mech.*, **53**, Part 4, 759–768.

Sutton, L. J., 1925: Haboobs. *Quart. J. Roy. Meteor. Soc.*, **51**, 25–30.

Tepper, M., 1950: A proposed mechanism of squall lines: The pressure jump line. *J. Meteor.*, **7**, 21–29.

——, 1955: On the generation of pressure jump lines by the impulsive addition of momentum to simple current systems. *J. Meteor.*, **12**, 287–297.

von Kármán, T., 1940: The engineer grapples with nonlinear problems. *Bull. Am. Math. Soc.*, **46**, 615–683.

Yih, Chia-Shun, 1969: *The Annual Review of Fluid Mechanics.* Annual Reviews, Inc., Palo Alto, Calif., 106 pp.